

Two Epochs of Globular Cluster Formation from Deep Fields Luminosity Functions: Implications for Reionization and the Milky Way Satellites

Harley Katz^{1*} and Massimo Ricotti^{1†}

¹*Department of Astronomy, University of Maryland, College Park, MD 20742, USA*

22 January 2018

ABSTRACT

The ages of globular clusters in our own Milky Way are known with precision of about ± 1 Gyr, hence their formation history at redshifts $z \gtrsim 3$ and their role in hierarchical cosmology and the reionization of the intergalactic medium remain relatively undetermined. Here we analyze the effect of globular cluster formation on the observed rest-frame UV luminosity functions (LFs) and UV continuum slopes of high redshift galaxies in the Hubble Ultra Deep Fields. We find that the majority of present day globular clusters have formed during two distinct epochs: at redshifts $z \sim 2 - 3$ and at redshifts $z \gtrsim 6$. The birth of proto-GC systems produce the steep, faint-end slopes of the galaxy LFs and, because the brightness of proto-GCs fades 5 Myrs after their formation, their blue colors are in excellent agreement with observations.

Our results suggest that: i) the bulk of the old globular cluster population with estimated ages $\gtrsim 12$ Gyr (about 50% of the total population), formed in the relatively massive dwarf galaxies at redshifts $z \gtrsim 6$; ii) proto-GC formation was an important mode of star formation in those dwarf galaxies, and likely dominated the reionization process. Another consequence of this scenario is that some of the most massive Milky Way satellites may be faint and yet undiscovered because tidal stripping of a dominant GC population precedes significant stripping of the dark matter halos of these satellites. This scenario may alleviate some remaining tensions between CDM simulations and observations.

Key words: (Galaxy:) globular clusters: general, galaxies: luminosity function, mass function, cosmology: theory

1 INTRODUCTION

Although globular clusters (GCs) are well studied in our local galactic neighborhood, their role in hierarchical cosmology and their formation history at redshifts $z > 3$, when the universe was less than ~ 2 Gyrs old, remains an unsolved problem. Several groups have attempted to model the formation of GCs using cosmological simulations (e.g., Griffen et al. 2010; Zonoozi et al. 2011), however, insufficient spatial resolution and a poor understanding of their initial mass function, as well as the mechanisms responsible for their formation leave many unanswered questions about their cosmological origin.

Nearly all GCs are compact self-gravitating star clusters fairly homogeneous in heavy elements (Snedden 2005). This suggests that most of their stars formed in a nearly

instantaneous burst with high efficiency of gas-to-star conversion (James et al. 2004; Carretta et al. 2009a). GCs are often classified into two categories: metal-poor with $[\text{Fe}/\text{H}] \leq -1.5$ and metal-rich with $[\text{Fe}/\text{H}] \geq -1.5$. The origin of these two populations is unknown, however this bimodal property has been observed in multiple galactic environments (Zepf & Ashman 1993). The ages of many Milky Way GCs and a few extra-galactic GCs have been estimated by analyzing the color-magnitude diagrams of the individual GCs. Vertical, ΔV , methods tend to have error bars of ~ 1 Gyr due to uncertainties in defining the precise main sequence turnoff, while horizontal methods, $\Delta(B-V)$, have similar error bars as a result of uncertainties in the theoretical model for the effective temperature T_{eff} of the stars (Sarajedini 2009). In addition, galactic metal poor GCs are older than metal rich GCs and have an age spread of approximately 1 Gyr, compared to the ~ 6 Gyr spread for metal rich GCs (Chaboyer et al. 1996; Rosenberg et al. 1999; Salaris & Weiss 2002;

* E-mail: hkatz@astro.umd.edu

† E-mail: ricotti@astro.umd.edu

De Angeli et al. 2005; Marín-Franch et al. 2009). The age gap between metal-poor and metal-rich GCs is greater than the range present within each individual population (Marín-Franch et al. 2009), suggesting that there are two distinct epochs of GC formation, adding to the complexity in modeling their formation and evolution history.

Assuming that the bulk of the old GC population formed around the epoch of reionization, Ricotti (2002) has shown that they would dominate the reionization process. Ricotti’s argument is simple: from the census of GCs in the present universe (estimated from the specific frequency of GCs), he derived the fraction of baryons in GCs and the number of ionizing photons per baryon per Hubble time they emitted (assuming they formed over a 1 Gyr period at $z \sim 6$). This number is likely to be a lower limit since most GCs have been destroyed or have been stripped of stars due to dynamical processes and stellar evolution (Ostriker & Gnedin 1997; Fall & Zhang 2001). Today, the fraction of stars in GCs today is negligible when compared to all of the stars in bulges and disks. However, at redshift $z \gtrsim 6$, only a small fraction of today’s stars existed, while many of today’s GCs, being the oldest known stellar systems, may have been present. Ricotti concluded that proto-GC formation may have been the dominant mode of star formation in primordial dwarf galaxies. In addition, because proto-GCs formed with a high star formation efficiency and are observed in the outer parts of dark matter halos, the UV radiation they radiate can more easily escape into the intergalactic medium (IGM) (Ricotti & Shull 2000), and contribute to the reionization process. Indeed, assuming a Salpeter IMF and UV escape fraction $f_{esc} \sim 1$, Ricotti showed that GC formation at $z \gtrsim 6$ can easily produce enough UV photons to reionize the universe.

The main uncertainty in this model is the fraction of the observed population of old GCs that formed at redshifts $z \gtrsim 6$. The epoch of reionization likely extended from $z \sim 14$ to $z \sim 7$ (Fan et al. 2006). The uncertainty on the age determination of old GCs prevents us from discriminating whether old GCs formed at redshift $z \sim 3 - 4$, after the epoch of reionization, or at redshift $z \sim 7 - 14$, thus contributing to reionization. In order to understand the role that GCs may have played during the reionization epoch, the formation history of the old GC population with estimated ages $\gtrsim 12 \pm 1$ Gyr (*i.e.*, formation redshift $z \gtrsim 4$) must be better constrained. In addition, constraining proto-GC formation at high redshift may be a key element to understanding the origin of the classical and ultra-faint Local Group dwarfs (Ricotti & Gnedin 2005; Bovill & Ricotti 2011a,b; Boylan-Kolchin et al. 2011).

Figure 1 (left) shows the distribution of the redshift of formation of the Milky Way GCs based on age measurement compiled by Forbes & Bridges (2010). The distribution shows that about 55% of Milky Way GCs are older than 12 Gyrs, thus formed at redshift $z > 4$. However, the errors on these ages are on the order of ± 1 Gyr. Assuming the worst case scenario where all of the GCs are 1 Gyr younger than the data suggests, 20% of Milky Way GCs would have still formed after redshift $z > 4$. The right panel of Figure 1 shows a Monte Carlo realization, consistent with observations of the redshift distribution (including Gaussian errors on the ages) of a bimodal population of GCs that form 20% of all clusters at $3 < z < 3.5$ and 80% at $5 < z < 5.5$. Due to

the large errors on the age measurements, is impossible to discriminate between different choices of the underlying GC bimodal distribution. For instance, a bimodal distribution with 45% of GC forming between $2.5 < z < 3$ and 55% at $6.5 < z < 7$, is statistically indistinguishable from the one shown in the figure.

The old stellar populations and compact size of present day GCs adds to the difficulty in detecting them beyond the Milky Way, even with our most powerful space telescopes. Kalirai et al. (2008) has identified bright unresolved sources surrounding the parent galaxy at $z = 0.0894$ in a Hubble space telescope (HST) image, which is one of the furthest known systems of old GCs at a luminosity distance of about 404 Mpc.

For about 5 – 10 Myrs after their formation, individual proto-GCs are extremely bright and have blue broad-band colors. In principle they are detectable with current instrumentation up to redshift $z \sim 7$ (see Section 3) and are certainly within the reach of even deeper near-IR observations which will be achieved with the James Webb space telescope (JWST) (Schaerer & Charbonnel 2011). Moreover, GCs are typically observed as systems of 3 – 10 GCs in dwarf galaxies (Puzia & Sharina 2008), to hundreds in more massive galaxies (the Milky Way has about 150 GCs and Andromeda about 500). With current space telescopes, proto-GC systems forming in high redshift dwarf galaxies are poorly resolved spatially. In Section 3.2 we show that they appear as blurred extended objects, brighter than an individual GC, since their formation is likely nearly coeval given the typical dynamical time scale of a few tens of Myrs in high- z dwarfs. These young proto-GC systems are therefore more easily detectable than sparsely distributed individual GCs in larger galaxies.

In this paper, we take an indirect approach to identifying the redshift of formation of GCs. We seek to constrain the largest number of proto-GCs that are allowed to form within any given redshift range, while remaining consistent with the observed UV luminosity functions (LFs) and colors of galaxies in the Hubble Ultra Deep Fields. We also produce simulated images of young proto-GC systems to lay the foundation for their direct identification with Wide Field Camera 3 (WFC3) on the HST and the Near Infrared Camera on the JWST.

This paper is organized as follows. In Section 2 we present basic calculations of the luminosity and mass budget of proto-GCs. In Section 3, we discuss the capabilities of the HST and the JWST in detecting and resolving young proto-GCs and present synthetic images of proto-GC systems based on observations of old GC systems in nearby dwarf galaxies by Puzia & Sharina (2008). In Section 4, we constrain the proto-GC formation rate at high- z by comparing observed LFs to simulated LFs of forming proto-GCs, and calculating the effect of proto-GCs formation on the UV continuum slope at 1500 Å. We present our results and discussion in Section 5 and the summary and conclusions in Section 6.

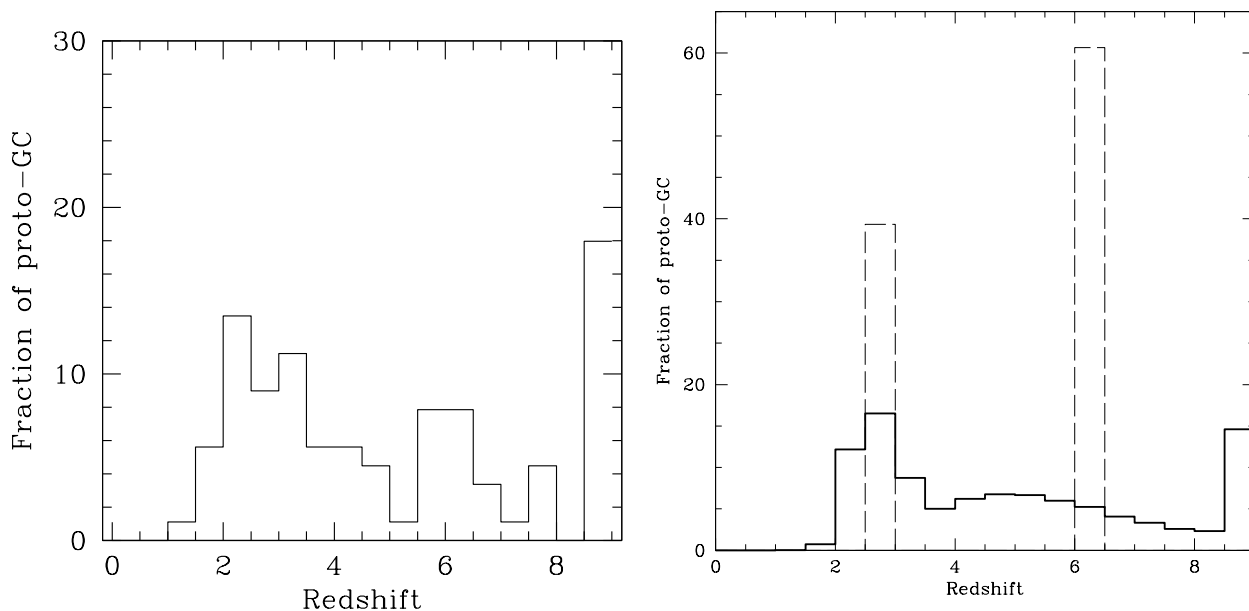


Figure 1. *Left.* Distribution of the redshift of formation of the Milky Way GCs based on age measurement from Forbes & Bridges (2010). The distribution is poorly known at $z > 3$ because the typical error on the ages of GCs is $\pm 0.5 - 1$ Gyr. *Right.* Monte Carlo realization of the redshift distribution (including errors on the ages) of a bimodal population of GCs that form 40% of all clusters at $3 < z < 3.5$ and 60% at $5 < z < 5.5$. Due to the large errors on the age measurements, it is impossible to discriminate between different choices for the underlying GC bimodal distribution. Most choices, as the one shown here, produce observed distributions broadly consistent with the Milky Way population of GCs.

2 BASIC CALCULATIONS AND ASSUMPTIONS

The mass distribution of present day GCs in the Milky Way is well described by a lognormal distribution with typical mass $M_{\text{obs}} \sim 1.4 \times 10^5 M_{\odot}$ (Shu et al. 2010). However, the initial masses of young proto-GCs, M_{ini} , were significantly larger than today’s observed masses, M_{obs} . Stellar evolution and dynamical effects, including galactic tides, dynamical friction and two-body relaxation (Ostriker & Gnedin 1997; Fall & Zhang 2001), significantly reduce the number and mean mass of young GCs from the epoch of formation to the present. Assuming a Salpeter initial mass function (IMF), Prieto & Gnedin (2008) found $f_{\text{di}} \equiv M_{\text{ini}}/M_{\text{obs}} \sim 9.1$. In their simulations they include the effects of stellar evolution, two-body relaxation, dynamical friction and tidal shocks as described by Fall & Zhang (2001). Simulations also show that the current mass distribution of GCs can be reproduced if the GC initial mass function (GCIMF) is either a power-law $dN/d\log M \propto M_{\text{ini}}^{-0.47}$ with $10^4 < M_{\text{ini}} < 10^7 M_{\odot}$ or a lognormal distribution with characteristic mass $M_{\text{ini}} = 1.5 \times 10^6 M_{\odot}$ (Shu et al. 2010).

Although the destruction rate and mass loss of GCs remains somewhat uncertain because these quantities are based on theoretical models with poorly known initial conditions (such as the IMF of stars in GCs, the GCIMF, and the formation sites of proto-GCs), recent observational developments on the stellar populations in GCs provide independent evidence for values of $f_{\text{di}} \sim 10 - 25$ (Schaerer & Charbonnel 2011). It is now clear that nearly all GCs exhibit large star-to-star variations of abundances in light elements (from C to Al), interpreted as a signature

of some degree of self-enrichment by gas pre-processed in short-lived, high mass stars (for details see, Gratton et al. 2001, 2004; Prantzos et al. 2007; Carretta et al. 2009b; Charbonnel 2010, and references therein). Self-enrichment models of GCs assume at least two populations of stars, with the first generation of massive stars polluting the second generation. The polluters are thought to be either massive AGB stars or fast rotating massive stars (Prantzos & Charbonnel 2006). These models, after assuming an IMF for the first generation stars, are constrained to reproduce the present proportion of first to second generation stars and their observed abundance patterns. Generally, all the models require the initial stellar masses of GCs to be considerably larger than their present day values (Prantzos & Charbonnel 2006; Decressin et al. 2007; D’Ercole et al. 2008; Decressin et al. 2010; Carretta et al. 2010). Schaefer & Charbonnel (2011), using the model of Decressin et al. (2007), have determined f_{di} as a function of the IMF of the first generation of stars. They found $f_{\text{di}} \sim 8 - 10$ in models in which the second generation stars are all retained by the GCs, and $f_{\text{di}} \sim 15 - 25$ in models in which second generation stars found in the Milky Way halo originate from the present-day population of GCs. This result is independent of, but in good agreement with the expectation from dynamical models (Prieto & Gnedin 2008). Thus, for the rest of this paper we will adopt a conservative fiducial value $f_{\text{di}} = 9.1$, at the lower end of the estimate by Schaefer & Charbonnel (2011). Note however that our results on constraining the formation rate of proto-GC systems do not depend on the assumed fiducial value for f_{di} .

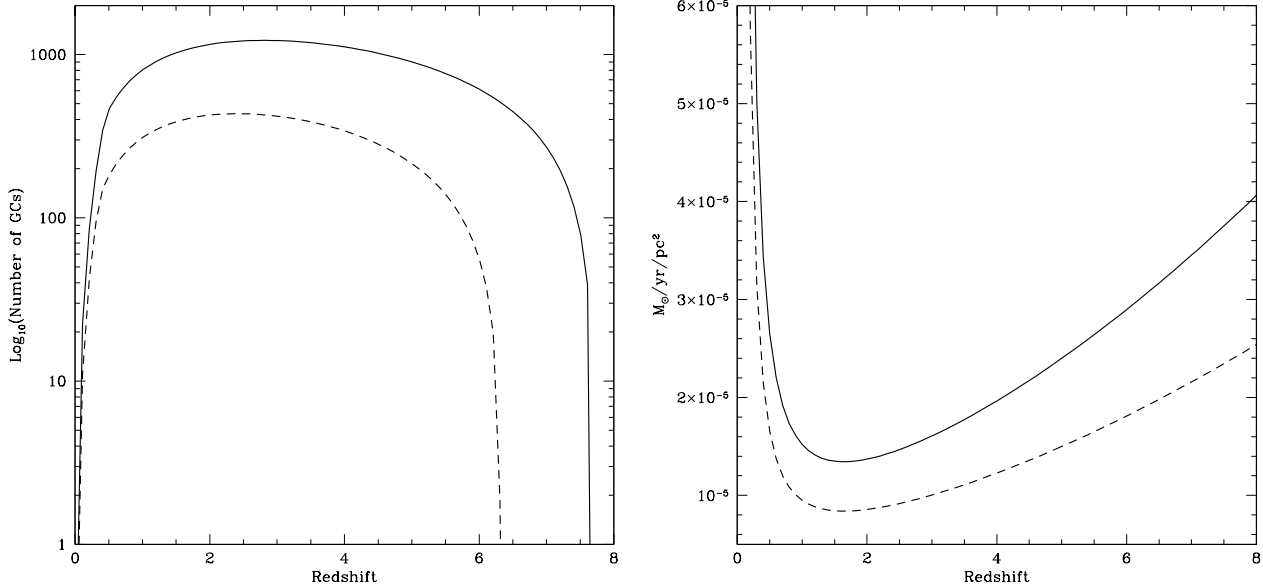


Figure 2. *Left.* The solid black line represents the average amount of GCs that the NIR camera on JWST would see as a function of redshift. The dashed line represents the average amount of GCs that the WFC on HST would see as a function of redshift. This assumes a limiting magnitude of 31 for JWST and 30.5 for HST. *Right.* The star formation rate per square parsec as observed with JWST is shown as the solid black line and the dashed line represents the same quantity as observed with HST.

2.1 Luminosity Function of proto-GCs

For a lognormal GCIMF, with a typical mass of $M_{ini} = 1.4 \times 10^6 M_{\odot}$, a young proto-GC is expected to have a peak UV magnitude at 1500 Å of $M_{AB} \approx -16.7$ at an age $< 5 - 10$ Myr. These GCs then fade by more than 4 mags due to stellar evolution (see e.g. models of Leitherer et al. (1999)). For a power law GCIMF, the most massive GCs have $M_{ini}^{max} \sim 10^7 M_{\odot}$ (Shu et al. 2010), corresponding to $M_{AB} \approx -19.3$. At redshifts of $z \sim 7 - 10$ this would correspond to a typical UV rest frame magnitude of $m_{AB} \sim 30.3$ at the peak of brightness, slightly fainter than the current detection limits of the deepest near-IR images taken with the WFC3 camera onboard of the HST (Bouwens et al. 2010).

2.2 Globular Cluster Formation Rate and Mass Budget

Using published data on the specific frequency of GCs in spiral, elliptical and dwarf galaxies, Ricotti (2002) estimated that about $\omega_{gc} \sim f_{di}(2.7 \times 10^{-4}) = 0.25\%$ of cosmic baryons have been converted into GC stars. Although this fraction is about 40 times smaller than today’s baryon fraction in stars (about 10%), it is likely a significant fraction of the collapsed baryons at redshifts $z \gtrsim 6$. Based on a compilation of observations of the present number of GCs in galaxies, Puzia & Sharina (2008) estimate an efficiency of GC formation in dark matter halos, $\eta_{dm} \sim 5.5 \times 10^{-5}$, defined as $M_{gc}^{tot} \equiv \eta_{dm} M_{dm}$ (assuming standard cosmological parameters $\Omega_b = 0.04$ and $\Omega_{dm} = 0.21$). Since at $z = 0$ most dark matter is in collapsed halos, the results of Puzia & Sharina (2008) imply $\omega_{gc} \equiv \eta_{dm} \Omega_b / \Omega_{dm} \sim 2.9 \times 10^{-4} f_{di}$, which is very good agreement with the value estimated by Ricotti (2002). Hereafter we will adopt a fiducial value for the mass

density of proto-GCs at formation:

$$\rho_{gc} \equiv \omega_{gc} \bar{\rho}_b \sim 1.35 \times 10^7 M_{\odot} \text{ Mpc}^{-3}, \quad (1)$$

where we have assumed $f_{di} = 9.1$ and the mean cosmic baryon density $\bar{\rho}_b = 5.51 \times 10^9 M_{\odot} \text{ Mpc}^{-3}$ (Komatsu et al. 2011).

It is easy to show that if even a small fraction $f_{gc} \sim 20\%$ of today’s GCs formed at redshift $z > 7$ (over a time interval $\Delta t = 0.5$ Gyr), the GC formation rate per comoving volume would be

$$\dot{\rho}_{gc} \approx f_{gc} \frac{\rho_{gc}}{\Delta t} \approx 0.54 \times 10^{-2} \left(\frac{f_{gc}}{20\%} \right) M_{\odot} \text{ yr}^{-1} \text{ Mpc}^{-3}, \quad (2)$$

comparable to the star formation rate density observed at redshift $z \sim 8$ (Bouwens et al. 2011). These simple estimates suggest that GC formation can be an important mode of star formation at high- z , and perhaps dominate the reionization process.

3 DETECTING PROTO-GLOBULAR CLUSTER SYSTEMS IN HUBBLE DEEP FIELDS

The planned launch of the JWST provides exciting prospects for our understanding of the high redshift universe. Here, assuming negligible dust extinction, we address the capabilities of both the HST and the JWST to detect young proto-GCs at high redshift. First, we estimate the absolute luminosity, number and morphology of young proto-GC systems in HST deep fields and make predictions for JWST deep fields.

The left panel in Figure 2 shows the number of GCs, N_{gc} , in the field of view of the Wide Field Camera (WFC)

on the HST (dashed line) and the Near Infrared Camera (NIR) on the JWST (solid line). For illustration purposes, we have assumed that half of all proto-GCs (after correcting for destruction), $f_{gc} = 50\%$, have formed in a single episode at redshift z . The value of N_{gc} is estimated as

$$N_{gc}(z) = 3\theta_A n_{gc} f_{lim}(z) \frac{D_L(z)}{1+z}, \quad (3)$$

where θ_A is the field of view of the camera, $D_L(z)$ is the luminosity distance at the redshift of interest, $f_{lim}(z)$ is the fraction of proto-GCs brighter than the limiting magnitude of the telescope at that redshift, and n_{gc} is the number density of GCs ($n_{gc} \approx 39.1 \text{ Mpc}^{-3}$ for a power law IMF and $n_{gc} \approx 33.8 \text{ Mpc}^{-3}$ for a lognormal IMF). Values of N_{gc} for different f_{gc} can be easily inferred by scaling the plot in Figure 2 (left). In principle, the WFC3 on the HST has the capabilities to detect proto-GCs with $M_{ini} = 10^7 M_\odot$ at redshifts up to $z = 7$ (see Section 3.2). However, such high mass clusters are only $f_{mag} \sim 0.8\%$ of the total (Shu et al. 2010). N_{gc} peaks at $z \sim 7 - 8$ because although the number of proto-GCs increases with redshift due to the larger volume in the field of view, the limiting magnitude of the instrument reduces the fraction of GCs that are detectable to the few most massive ones. In conclusion, single proto-GCs during their youth are detectable with current instrumentation up to $z \sim 6$, and are certainly well within the reach of deeper near-IR observations which will be achieved with the JWST. Although we cannot spatially resolve these sources at high redshifts, their presence in WFC and NIR images may be significant when compared to the number of high-redshift galaxy candidates.

3.1 GCs Versus Host Galaxy Surface Brightness

Using the average half light radius calculated from the Fornax Cluster Survey VII (Masters et al. 2010), of $2.8 \pm 0.3 \text{ pc}$ for red GCs and $3.4 \pm 0.3 \text{ pc}$ for blue GCs, the maximum redshifts that WFC and NIRcam can resolve these systems are $z = 0.0028$ (11.9 Mpc) and $z = 0.0072$ (30.7 Mpc), respectively. Without adaptive optics from the ground it is impossible to resolve or take a spectrum of GCs at intermediate and high redshifts. Thus, because of their high star formation rate at formation, GCs will appear as especially bright point sources surrounding their host galaxies and for about 5-10 Myrs from formation they may outshine their host galaxies. A GC of $10^7 M_\odot$, with a half light radius of 3.4 pc that forms all of its stars in $\sim 10 \text{ Myr}$, will have a SFR per unit area of $\dot{\Sigma}_{gc} \approx 2.75 \times 10^{-2} M_\odot \text{ yr}^{-1} \text{ pc}^{-2}$. However, since the proto-GC is unresolved the effective SFR per unit area depends on the pixel size of the detector, and at redshift $z = 6$ is $\dot{\Sigma}_{gc}^{eff} \approx 1.81 \times 10^{-5} M_\odot \text{ yr}^{-1} \text{ pc}^{-2}$ for the WFC on the HST. As a comparison, the bulge of the Milky Way, which has a mass of approximately $2 \times 10^{10} M_\odot$ within a radius $\sim 3 \text{ kpc}$, assuming its stars forms over 1 Gyr, would have a SFR per unit area of $\dot{\Sigma}_* \approx 2.83 \times 10^{-6} M_\odot \text{ yr}^{-1} \text{ pc}^{-2}$. The Large Magellanic Cloud (which we are using to compare GCs to dwarf galaxies) has a mass of $3 \times 10^{10} M_\odot$ with an effective radius of 5 kpc. Assuming a continuous SFR over 1 Gyr, we infer a SFR per unit area of $\dot{\Sigma}_* \approx 3.82 \times 10^{-7} M_\odot \text{ yr}^{-1} \text{ pc}^{-2}$. Figure 2 (right) shows the effective SFR per unit area of forming proto-GCs as a function of redshift and for two different proto-GC masses. Because

proto-GCs are unresolved, with increasing redshift their effective surface brightness increases due to the increase of the angular resolution. Assuming that proto-GCs systems are poorly spatially resolved and that their formation is synchronized to within 10 Myr as described later, we expect that the light from a high- z dwarf galaxy will be dominated by the proto-GC system for about 10 Myr after their formation.

3.2 Simulated Images

The best constraint on proto-GC formation at high redshift is their direct detection. As discussed in Section 3, the large star formation rates and compact sizes of proto-GCs allow them to outshine their host galaxies for a brief time. Figure 3 shows simulated images of proto-GC systems for 1 Msec observations with HST and JWST at different redshifts, and for two different choices of the host galaxy mass. To generate the images, we have used data on old GC systems observed in a survey of nearby spheroidal and irregular dwarf galaxies (Puzia & Sharina 2008). We randomly generate systems of GCs around these types of dwarf galaxies, modeled after the number of GCs, and the magnitude and structural data of the host galaxy. We randomly select a radius, determined by averaging the volumes of shells in which GCs orbit around eight different dwarf irregular galaxies. We then project on the sky the GC position. The magnitude of each GC is also randomly assigned in a range of three magnitude bins from $-18 < M_{AB} < -15$. We use the theoretical point spread function to convolve the point source over many pixels. Next, the three-dimensional positions of these systems were projected onto a two dimensional image with an arbitrary viewpoint and applied a normalized gray scale that attributes relative brightness to the proto-GCs. We include the background noise with signal to noise ratios of the 1 Msec exposure on each camera (consistent with that of the HUDF).

The brightness of the most massive proto-GCs is at the detection limit for the two space telescopes. Because of this, the signal to noise ratio of these systems is low and it might often be impossible to extract these systems over the background noise. Additionally, the theoretical images demonstrate that at around $z = 1$, the systems of GCs tend to produce an extended source rather than be resolved as distinct objects. This may effect the observers ability to differentiate between GC systems and the host galaxy all the way up to $z = 4$. Furthermore, if the systems form in groups rather than individually, this effect may be amplified and further limit the ability of an observer to identify GC systems. However, at $z > 4$, this effect will be significantly reduced and the probability of observing individual GCs or GC's in groups is far greater.

4 CONSTRAINING THE PROTO-GC FORMATION RATE AT HIGH-Z WITH UV LUMINOSITY FUNCTIONS AND CONTINUUM SLOPES

In this section we calculate the effect of the formation of proto-GCs on the observed high- z UV luminosity functions

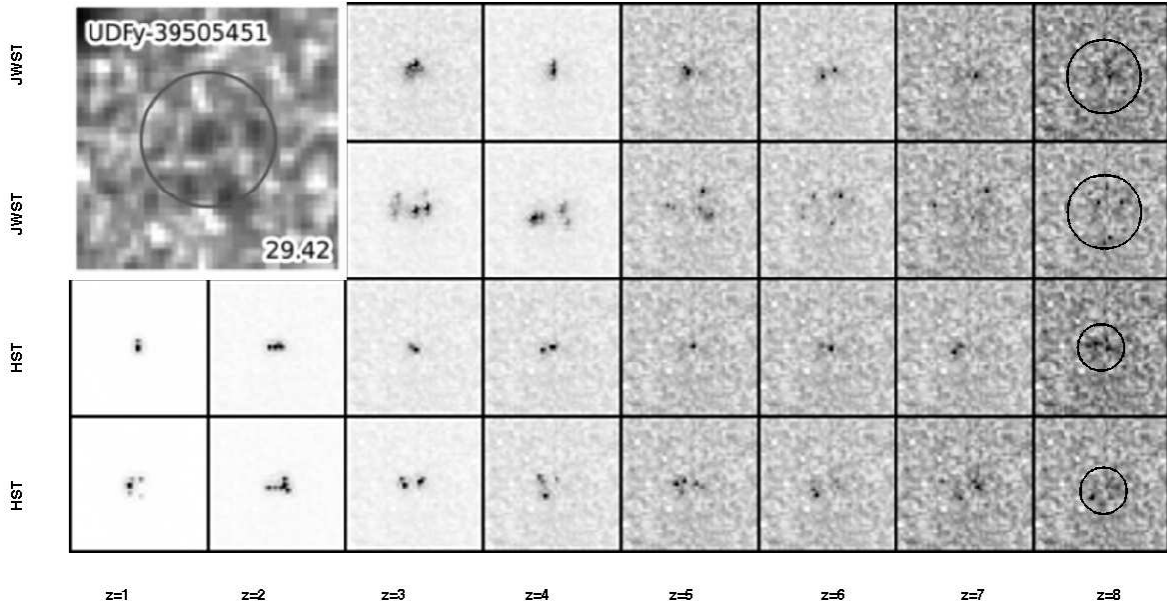


Figure 3. The top rows are the theoretical images from the WFC on HST and the bottom rows are the theoretical images from the NIRcam on JWST. These were computed to model a total exposure time of 1,000,000 seconds to be consistent with the HUDF. HST sensitivity extends from $z = 0 - 8$ from the UV and IR imaging equipment, while JWST only has sensitivity higher than $z = 2.33$ for 1500 Å. At the higher redshift we can see that the individual GCs are more identifiable. PSFs for JWST were found in the simulated PSF library provided by STScI while the HST PSFs were generated with the Tiny Tim software. Shown at the top left is an actual image from Bouwens et al. (2011). We use this to show a comparison of an actual $z = 8$ candidate that appears to be multiple sources with the multiple source images that we have generated.

(LF). The basic idea is to build synthetic luminosity functions, assuming that the GC system outshines the other stellar populations in the galaxy during the first 5-10 Myr after its formation. We use data from Bouwens et al. (2011) for LFs at redshifts $z > 7$, Bouwens et al. (2007) for the B, V, and I dropout LFs, and Oesch et al. (2010) for the $z = 1.5, 1.9$, and 2.5 LFs.

4.1 Unresolved proto-GCs

Our first approach is to consider the formation of individual proto-GCs. Although not the most realistic, this case is the simplest and nearly model independent. Physically, this approach corresponds to a scenario in which the formation of the proto-GC system in a dark matter halo is not synchronized to within a few tens of Myrs, or the most luminous proto-GC outshines all the others. This is the most conservative assumption but is less appropriate at redshifts $z \gtrsim 6$ when the typical dynamical times in virialized halos are short:

$$t_{dyn} \equiv \frac{R_s}{v_{vir}} \approx 11 \text{ Myr} \left(\frac{1 + z_{vir}}{10} \right)^{-1.5}, \quad (4)$$

where $R_s \simeq R_{vir}/5$ and v_{vir} are the scale radius and the virial velocity of the halo, respectively. We have adopted two choices of the initial mass functions of proto-GCs (GCIMF): a lognormal and power-law (see § 2), both reproducing the present day GC mass function in the Milky Way (Shu et al. 2010). Both choices produce nearly identical constraints.

In order to calculate the proto-GCs LFs, as a first order approximation we assume that GCs form in a short burst with $\Delta t_{form} \lesssim 10$ Myr (instantaneous mode of star

formation). Using Starburst-99 (Leitherer et al. 1999) we derive the evolution of the absolute magnitude of proto-GCs and their color (parameterized by β , the log-slope of the spectrum at 1500 Å) as a function of time from the burst. Proto-GCs produce the majority of their radiation in the UV band in the first 5 – 10 Myr of their life, before rapidly evolving to higher magnitudes. We compute the fraction $p_{gc}(M_{gc})$ of GCs that form in each log mass bin, using constant log bin spacing of $0.2 M_\odot$, spanning from $10^4 M_\odot$ to $10^{7.2} M_\odot$ for the power-law GCIMF and from $10^{3.2} M_\odot$ to $10^{7.4} M_\odot$ for the lognormal GCIMF. The number of GCs at peak luminosity per unit comoving volume is $n_{gc}(M_{gc}) = f_{gc} f_{on} \rho_{gc} p_{gc} / M_{gc}$, where $f_{gc}(z)$, the fraction of proto-GCs forming in each redshift bin, is the free parameter we wish to constrain. Here, f_{on} is the fraction of time the proto-GC is at peak luminosity which is about $f_{on} \equiv 10 \text{ Myr} / \delta T_z$, where δT_z is the time interval corresponding to the characteristic redshift depth of the observed luminosity function. Finally, we compute the luminosity function ϕ_{gc} from the proto-GC mass function converting from stellar masses to magnitudes (using Starburst-99 for an instantaneous burst).

In order to account for the evolution of GCs to higher magnitudes as they age, we apply a correction to the calculation of the LFs. Proto-GCs after the first 5-10 Myrs become fainter and redder, but their number in each redshift bin is larger because they remain at fainter magnitudes a longer time. We use Starburst-99 to determine the time Δt a proto-GCs of constant mass has a given magnitude. The number of GCs at fainter magnitudes from the peak is obtained analogously to the calculation above but with $f_{on} = \Delta t / \Delta T_z$.

Thus, after converting proto-GCs masses to magnitudes, we integrate over a time interval ΔT_z .

Figure 4 (left) shows the UV LFs of (individual) proto-GCs (dotted lines) compared to the observed LFs in the HUDF at different redshift intervals. The normalization of the proto-GCs LF in each redshift bin is proportional to the parameter f_{gc} , that we want to constrain. The proto-GCs LFs have steeper faint-end slopes than the observed LFs, hence we are able to set upper limits on f_{gc} . The values of f_{gc} for each redshift bin are reported in Table 5.

4.1.1 Effective UV Continuum Slopes

Once we have constrained f_{gc} using the observed LFs, we analyze the effect of GC formation on the UV continuum slope at 1500 Å. Proto-GCs with ages $< 5 - 10$ Myr have UV continuum slope $\beta = -2.69$ (Leitherer et al. 1999). We evolve the higher mass GCs into the lower luminosity bins, as was described when comparing the luminosity functions, and compute the weighted average of the β at half magnitude steps with respect to an arbitrary initial absolute magnitude. To determine the effective color, we set $\beta_{eff} = f(\beta_{gc} - \beta) + \beta$, β_{gc} is the color parameter from the GCs and β are the observed mean values of deep field galaxies described by Bouwens et al. (2009), and f is the fractional influence of the GCs on the UV continuum slope. In order to constrain the maximum percentage of GC formation, we first measure f , the ratio of the proto-GC LF ϕ_{gc} to the observed LF ϕ_{gal} . We then apply this ratio to the corresponding bin in the UV continuum slope and determine whether this maximum percentage can be further constrained by a new fraction f_β . Finally, we multiply the old GC percentage by f_β to obtain our new constraint. In Figure 4 (right), β_{eff} is compared to the the current values of the UV continuum slope. Because of the limited range of the UV continuum slope at the faint end we extrapolate the least squares fit yet remain conservative in constraining f_β estimates. When comparing β_{eff} to the known UV continuum slope with the Power Law and Gaussian models where GCs form in groups of ten, we can constrain the maximum percentage of GC formation to a higher degree of accuracy by noting where β_{eff} deviates from the error bars recorded by Bouwens et al. (2009).

4.2 Unresolved Proto-GC Systems

The second approach considers that more than one proto-GC forms in each host galaxy, and as discussed in Section 3.2, observations measure the integrated light from the proto-GC system. In this second case, we do not need to know the GCIMF, but the efficiency of proto-GC formation as a function of the mass of the host galaxy. We build on the results from Puzia & Sharina (2008) that the mass in GCs $M_{gc,tot}$ in a large sample of local dwarf galaxies is proportional to the total host halo mass M_{dm} within the luminous radius of the galaxy: $M_{gc,tot}(z=0) = \eta_{dm}(z=0)M_{dm}(z=0)$ with $\eta_{dm}(z=0) = 5.5 \times 10^{-5}$. However, this relationship is only measured at $z=0$ and does not take into account evolutionary effects such as galaxy mergers, proto-GC formation and disruption as a function of time. For instance, we know that only a fraction $f_{di}(M_{dm}, z) \leq 1$ of proto-GCs

have survived to the present. Thus, we assume that

$$M_{gc,tot}(z) = \eta_{dm}(z)M_{dm}(z), \quad (5)$$

where $\eta_{dm}(z)$ is the parameter we wish to constrain.

Modeling GC systems in dark matter halos is somewhat model dependent as the shape of the luminosity function depends on the range of halo masses in which proto-GCs form. However, we find that the only parameter that significantly affects the luminosity function is the mass of the smallest dark matter halos allowed to form GCs. Our model assumptions are as follows. We assume a constant efficiency of GC formation as a function of the halo mass $\eta_{dm}(z)$ for $M_{dm}^{min} < M_{dm} < M_{dm}^{max}$, and no globular cluster formation outside this halo mass range. We use the Press-Schechter formalism to obtain the mass function of dark matter halos as a function of redshift dn_{halo}/dM_{dm} , then convert dark halo masses to the masses of proto-GCs systems using Equation (5). Finally, we calculate the luminosity function by converting the total proto-GC mass to luminosity using Starburst 99 as described in § 4.1. As discussed in the previous here we also include the effect of aged GCs that form within the redshift bin under consideration and in the higher redshift bins (note that at high- z there is little time for GCs to age significantly and become redder).

The proto-GC LF is not sensitive to M_{dm}^{max} , that we hence assume larger than the exponential cut-off mass-scale in the Press-Schechter mass function. We instead find that the results are sensitive to M_{dm}^{min} , or equivalently to the virial temperature of the halo T_{vir}^{min} . Hence, we explore the results assuming 4 different values of $T_{vir}^{min} = 5 \times 10^4, 8 \times 10^4, 10^5$ K and 1.5×10^5 K. In each model we vary the value of $\eta_{dm}(z)$ to be consistent with observations of the LFs and colors in each redshift bin, similarly to what was done for single proto-GCs. The main difference here is that varying η_{dm} shifts the proto-GCs LF horizontally along the magnitude axis, while for single proto-GCs the free parameter f_{gc} had an effect on the overall normalization of the LF (shift along the y-axis).

Figure 5 (left) shows the LF for proto-GCs systems (dotted line) compared to observed deep field galaxies LFs (solid lines) in different redshift bins. In each panel, corresponding to a different redshift, we have used a value of $\eta_{dm}(z)$ that maximizes the contribution of the proto-GC luminosity function to the observed LF remaining consistent with observations. We also repeat the same procedure described in Section 4.1.1 to further constrain $\eta_{dm}(z)$ from the UV colors of observed deep field galaxies. Figure 5 (right) shows the UV colors of proto-GCs systems, β_{gc} (dotted lines) and the effective galaxies UV colors, β_{eff} (dashed lines), compared to observations (solid lines and points with error bars). The curves in the figure are for the largest values of $\eta_{dm}(z)$ consistent with observations.

The values of $\eta_{dm}(z)$ constrained by the data allows us to calculate $\rho_{gc}(z) = \bar{\rho}_b \eta_{dm} \omega_{halos}$, where ω_{halos} is the fraction of collapsed dark matter in halos with $M_{dm}^{min} < M_{dm} < M_{dm}^{max}$ for each observed redshift bin of depth $\Delta t(z)$. From ρ_{gc} we derive the upper limits on the proto-GC formation rate $\dot{\rho}_{gc}(z) \approx \rho_{gc}(z)/\Delta t(z)$ and hence upper limits on $f_{gc}(z)$. The results are shown in Table 5 for our four model assumptions and are summarized in Figure 6 (left).

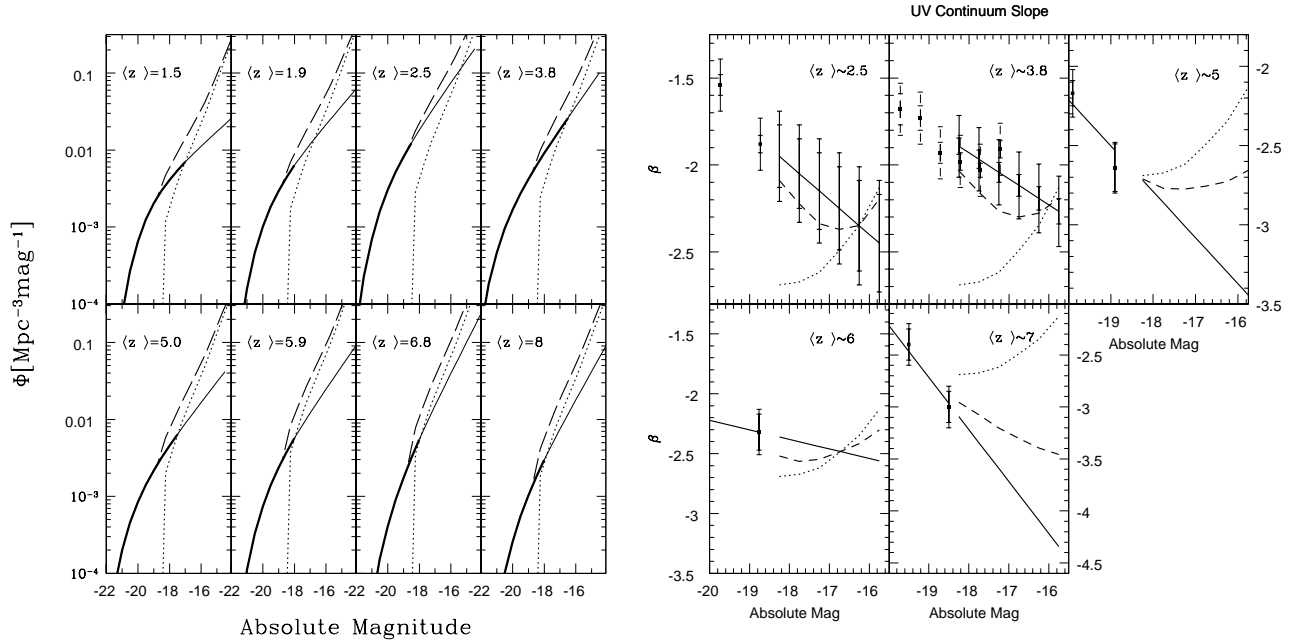


Figure 4. *Left.* The UV Luminosity Functions from Oesch et al. (2010) ($z = 1.5, 1.9, 2.5$), Bouwens et al. (2007) ($z = 3.8, 5.0, 5.9$), and Bouwens et al. (2011) ($z = 6.8, 8$) are shown as the thick black line. The observed luminosity function is only shown to the limiting magnitude of the observational data. The dotted lines show the LF of a fraction f_{gc} of proto-GCs forming in the same redshift bin as the observations, assuming a power law GCIMF. The long-dashed line represents the sum of the proto-GCs LFs and observed LFs. *Right.* The UV continuum slopes for the individual GC formation model. The observational UV continuum slopes are shown with the solid lines as the least squares slopes. The least squares fits are only shown with error bars if they were provided by the literature and extrapolations are shown with a gap. Raw data points and accompanying error bars are also shown from Bouwens et al. (2009) and Bouwens et al. (2011). The dotted lines are the theoretical UV continuum slopes for forming GCs and the dashed lines are the β_{eff} slopes.

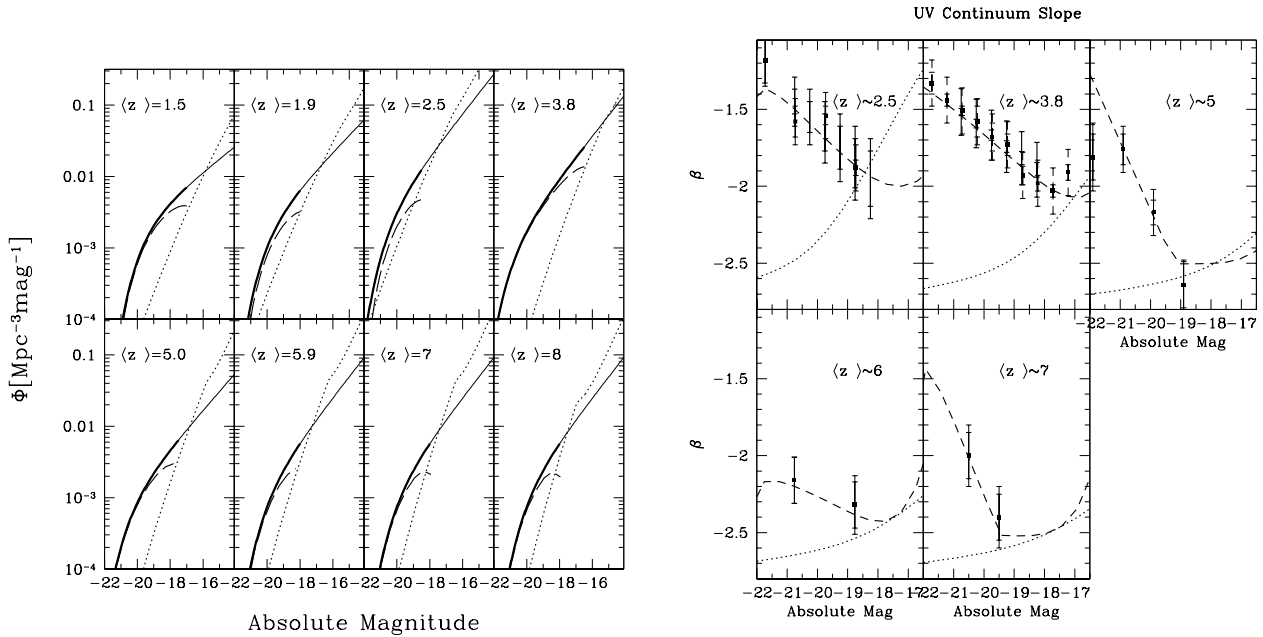


Figure 5. The left and the right panels are analogous to the ones in Figure 4 but for systems of proto-GCs allowed to form in halos with virial temperature $T_{vir} > 5 \times 10^4$ K. The long dashed lines show the difference between the observed LFs and the proto-GCs LFs.

Table 1. Constraints on globular clusters formation efficiency from LFs and UV colors. For proto-GCs systems we have assumed $T_{vir} > 5 \times 10^4$ K.

$\langle z \rangle$	t[Gyr]	dt[Gyr]	f_{gc} Single GCs		$\eta_{dm}(z)/5.5 \times 10^{-5}$ Systems of GCs	
			LF	LF+color	LF	LF+color
1.5	9.320	0.99	75%	–	0.23	–
1.9	10.155	0.92	100%	–	0.79	–
2.5	10.999	0.56	100%	100%	2.56	0.77
3.8	11.995	0.36	55%	30%	1.00	1.00
5.0	12.469	0.28	35%	21%	2.08	1.04
5.9	12.695	0.17	40%	24%	4.08	4.08
6.8	12.858	0.13	28%	11%	7.38	7.38
8.0	13.014	0.14	15%	–	14.46	–

Table 2. Upper limits on globular clusters star formation rate ($M_{\odot}/yr/Mpc^3$)

z	$T_{vir} > 1.5 \times 10^5 K$	$T_{vir} > 1.0 \times 10^5 K$	$T_{vir} > 8.0 \times 10^4 K$	$T_{vir} > 5.0 \times 10^4 K$
4.25	0.0063	0.0061	0.0055	0.0051
4.75	0.0048	0.0050	0.0035	0.0032
5.25	0.0042	0.0067	0.0052	0.0073
5.75	0.0050	0.0100	0.0095	0.0151
6.25	0.0061	0.0105	0.0118	0.0181
6.75	0.0069	0.0082	0.0112	0.0162
7.25	0.0067	0.0060	0.0095	0.0144
7.75	0.0055	0.0051	0.0075	0.0146
8.25	0.0041	0.0046	0.0054	0.0155
8.75	0.0026	0.0041	0.0033	0.0164

5 RESULTS AND DISCUSSION

The upper limits on the proto-GC formation rate from the Hubble deep fields are summarized in Table 5 and in Figure 6. The table shows the constraints from the observed LFs and UV colors at 1500 \AA (parameter β) of high- z galaxies, for both single proto-GCs and systems of proto-GCs.

Strong constraints are possible because the proto-GC LFs have a faint-end slope generally steeper than observed, and their spectral slope at 1500 \AA is typically bluer than observed ($\beta \sim -2.7$). This is because the instantaneous burst of star formation of proto-GCs and the subsequent rapid time evolution of their luminosity from bright to faint, steepens the LF with respect to the intrinsic slope of the GCIMF (for single proto-GCs). However, for systems of proto-GCs the faint-end slope of the LF depends on the slope of the halo mass function, and thus depends on the masses of the proto-GC host halos and their redshifts of virialization. This is why, for GC systems, the limits are sensitive to the assumed minimum mass of halos that can host proto-GCs.

At high- z the limits on the formation rate of proto-GC systems are the most stringent. These, in combination with the measured ages of GCs in the Milky Way that instead constrain best their lower redshift formation rate, allow us to conclude that there are two distinct epochs of proto-GC formation: one at $z \sim 2.5$ near the peak of the global SFR density in the universe, and one before or around the reionization epoch. Figure 6 (left) shows the upper limits on the GCs formation rate (top panel), the proto-GC redshift distribution (middle panel) and the cumulative proto-GC redshift distribution (bottom panel)

from the combined constraints from the LF and colors discussed in the previous section. In addition, the proto-GC redshift distribution and cumulative distributions are constrained¹ at redshifts $z < 3$ by the measured ages of Milky Way GCs from Forbes & Bridges (2010). The lines in Figure 6 (left) correspond to different assumptions on the minimum mass of the halos in which proto-GC systems form: $T_{vir} > 5 \times 10^4$ K (dashed line), $T_{vir} > 8 \times 10^4$ K (dotted line); and $T_{vir} > 1.5 \times 10^5$ K (solid line). The limits on the GCs formation rate are independent of the assumed fiducial value for ρ_{gc} , while the redshift distribution and cumulative redshift distribution of GC are normalized to ρ_{gc} (that is somewhat uncertain as it depends on f_{di}). Because of the uncertainty on f_{di} and because the lines represent upper limits, the cumulative GC distribution may not be normalized to unity.

Although our results only set upper limits on the GC formation rate, at redshifts $z \gtrsim 6$ the LFs and colors of simulated proto-GC systems are in good agreement with observations, suggesting that a large fraction of high redshift galaxies have a star formation mode compatible with proto-GC formation. Moreover, the upper limit on the cumulative distribution of proto-GCs normalized to ρ_{gc} approaches unity, also suggesting that the upper limits are close to the actual values of the distribution. We also note that even a small fraction (10-20%) of present-day GCs forming at $z \gtrsim 6$ accounts for a significant fraction of the total star formation

¹ This constrain implicitly assumes that Milky Way GCs accurately describe the age distribution of the GC population in the rest of the Universe.

activity at high redshift. Our model shows that if proto-GCs are allowed to form in halos with $T_{\text{vir}} \gtrsim 5 \times 10^4$ K (dashed lines), current deep fields are missing a significant fraction of the global SFR because of the steep faint-end slope of the LF.

Finally, we re-assess the possibility that proto-GCs may be dominant sources of IGM reionization (Ricotti 2002). The high star formation efficiency of young proto-GCs and their location in the outer parts of galaxies both point to a high escape fraction of the ionizing radiation they emit. Figure 6 (right) shows the upper limits on the number \mathcal{N} of ionizing photons emitted per Hubble time per baryon by proto-GC formation, assuming $f_{\text{esc}} = 1$. The meaning of the lines is the same as in the left panel. A value of $\mathcal{N} \sim 5$ is sufficient for reionizing the IGM and keeping it ionized (Miralda-Escudé et al. 2000). This scenario is especially interesting in light of current studies that are trying to identify the sources of reionization in deep surveys at $z \sim 7-8$, finding that the sources of reionization must be faint and thus relatively numerous (Bouwens et al. 2010).

6 SUMMARY AND CONCLUSIONS

Present day GCs are difficult to observe beyond the Milky Way because their stellar populations are very old and faint. All their bright massive stars have evolved beyond the main sequence and the surviving clusters have lost a significant fraction of their lower mass stars due to dynamical effects (tides, two-body relaxation, dynamical friction). However, during the first 5-10 Myr after their formation, proto-GCs were extremely bright, with the most massive GCs reaching absolute magnitudes of $M_V \approx -19$. This is due to their high-efficiency of star formation and their relatively large total mass at formation that can be estimated about 5-10 times larger than their current stellar mass [although this number is uncertain, depending on dynamical effects (Ostriker & Gnedin 1997) as well as the IMF of their stars (Schaerer & Charbonnel 2011)].

In this paper we have shown that the most massive proto-GCs are detectable in the HUDF and will be detectable by the JWST up to redshift $z \sim 8$, when imaged at their peak luminosity. In addition, since GCs are found with a high specific frequency in present day dwarf galaxies (5-10 within of a few kpc from the dwarf center), and we expect their formation to be synchronized to within ~ 10 Myrs, such proto-GC systems appear a poorly resolved high redshift galaxy with multiple knots of star formation. The short dynamical time scales in primordial dwarf galaxies support this scenario. However, because proto-GCs maintain their peak luminosity for a very small fraction of the Hubble time, their numbers are small within the limited field of view of deep HST and JWST images, especially if a large fraction of them form at low redshifts when the Hubble time is large. But if a non-negligible fraction of today's GCs have formed at redshifts $z > 3$, they are detectable in the HUDF and will contribute a substantial fraction of the high redshift stellar populations and to IGM reionization, as first noted by Ricotti (2002).

Our present work has shown that only a small fraction of the present-day GCs populations could have formed in the redshift range $3 < z < 5$, because otherwise they would af-

fect significantly and be inconsistent with the observed LFs and the colors at 1500 Å of high- z galaxies in the HUDF. In addition, given the age estimates of Milky Way GCs, a significant old population that formed at $z > 3$ must exist (even if we take into account the large errors on their age estimate from color-magnitude methods). We conclude that the bulk of the old GC population with estimated ages $\gtrsim 12$ Gyr, roughly 50% of the total, formed in the most massive dwarf galaxies at redshifts $z \gtrsim 6$ and that proto-GC formation, an important mode of star formation in some primordial dwarf galaxies, likely dominated the reionization process.

Although our study only sets upper limits on the formation rate of proto-GCs, the steep faint-end slope of the LFs and the blue colors of $z \sim 7-8$ galaxy candidates in the HUDF are consistent with a significant fraction of their stellar populations being proto-GCs. The simulated images of systems of proto-GCs forming in $z \sim 7-8$ dwarf galaxies present remarkable morphological similarities with some of the observed candidates. JWST will be able to detect and image this population that is likely responsible for the reionization of the universe, to higher redshifts and fainter magnitudes.

Finally, we speculate that if GC formation was a dominant mode of star formation in some dwarf galaxies, this may have implications to understanding some unsolved issues regarding the Milky Way satellites. Bovill & Ricotti (2009) have pointed out that many of the ultra-faint Milky Way satellites have properties that are consistent with being the fossil remnants of the first dwarf galaxies formed before reionization. But they also noted that a problem remains regarding an apparent lack of massive and bright satellites that cannot be reconciled by simply populating the most massive sub-halos with luminous satellites using monotonic luminosity-to-mass matching methods (Bovill & Ricotti 2011a,b). Boylan-Kolchin et al. (2011) have also suggested a possible problem with the density of the most massive Milky Way satellites that seems inconsistent with dark matter Λ CDM simulations (neglecting baryonic physics). Solutions to this second problem include SN feedback processes that may reduce the central density of satellites, and statistical arguments involving a better knowledge of the mass and circular velocity of the Milky Way. However, these two solutions would not solve the problem emerging from Bovill & Ricotti (2011b) work.

A solution that would reconcile both results is to assume that classical dwarfs do not reside in the most massive dark matter satellites. This is possible only if the most massive satellites of the Milky Way are darker than some of the least massive (*i.e.*, a non-monotonic mass-to-light ratio). There are two ways to achieve this result: i) suppress star formation preferentially in the most massive satellite progenitors, with a feedback process such as photoheating by AGN etc.; or ii) remove most of its stars without removing most of the dark matter. This second proposal seems implausible if stars are concentrated at the center of the dark matter halo. However, if star formation in some of the most massive surviving Milky Way satellites was dominated by proto-GC formation in the outskirts of their dark matter halo (as observed in nearby dwarf galaxies), tidal stripping of their GC systems may significantly reduce their luminosity without destroying the dark halo, thus explaining their apparent darkness. Examples of galaxies with stellar popu-

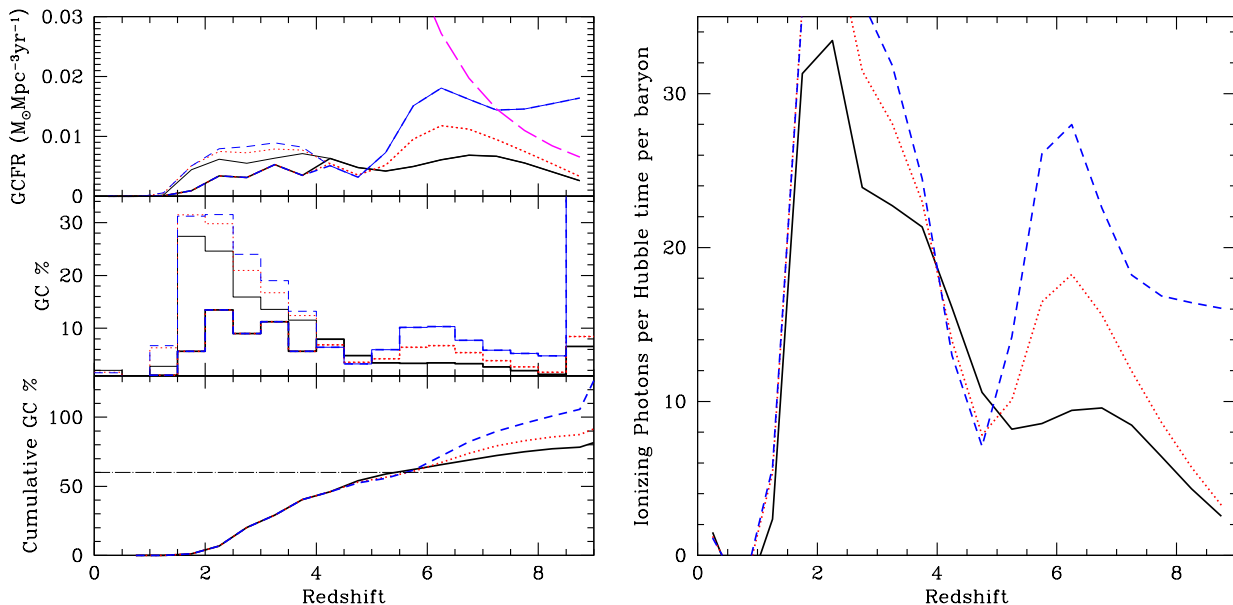


Figure 6. *Left.* Upper limits on the GC formation rate as a function of redshift from LF and color constraints for systems of GCs (see text). The top panel shows the GC formation rate compared to the observed SFR (long-dashed line), the middle panel shows the distribution of formation redshifts of GCs and the bottom panel shows the cumulative distribution. The different lines correspond to different assumptions on the minimum virial temperature the host halos in which GC systems are allowed to form: $T_{\text{vir}} > 5 \times 10^4 \text{ K}$ (dashed line); $T_{\text{vir}} > 8 \times 10^4 \text{ K}$ (dotted line) $T_{\text{vir}} > 1.5 \times 10^5 \text{ K}$ (solid line). The thick lines include the constraints at low-redshift from estimated GCs ages. *Right.* Upper limits on the ionization rate per Hubble time per baryon from GCs. The lines correspond to the GCs formation rates as in the left panel.

lations clearly dominated by GCs have not been identified in isolation in the local universe, but their formation might be biased, such that today they have mostly merged into massive galaxies. Another possibility is that isolated massive dwarfs were once dominated by GC systems but have accreted gas and formed new stars at later times (Ricotti 2009), while the ones that merged into the Milky Way did not experience further star formation.

REFERENCES

- Bouwens, R. J., Illingworth, G. D., Franx, M., Chary, R.-R., Meurer, G. R., Conselice, C. J., Ford, H., Giavalisco, M., & van Dokkum, P. 2009, *ApJ*, 705, 936
- Bouwens, R. J., Illingworth, G. D., Franx, M., & Ford, H. 2007, *ApJ*, 670, 928
- Bouwens, R. J., Illingworth, G. D., Oesch, P. A., Labbé, I., Trenti, M., van Dokkum, P., Franx, M., Stiavelli, M., Carollo, C. M., Magee, D., & Gonzalez, V. 2011, *ApJ*, 737, 90
- Bouwens, R. J., Illingworth, G. D., Oesch, P. A., Trenti, M., Stiavelli, M., Carollo, C. M., Franx, M., van Dokkum, P. G., Labbé, I., & Magee, D. 2010, *ApJ*, 708, L69
- Bovill, M. S. & Ricotti, M. 2009, *ApJ*, 693, 1859
- . 2011a, *ApJ*, 741, 17
- . 2011b, *ApJ*, 741, 18
- Boylan-Kolchin, M., Bullock, J. S., & Kaplinghat, M. 2011, *MNRAS*, 415, L40
- Carretta, E., Bragaglia, A., Gratton, R., D’Orazi, V., & Lucatello, S. 2009a, *A&A*, 508, 695
- Carretta, E., Bragaglia, A., Gratton, R., & Lucatello, S. 2009b, *A&A*, 505, 139
- Carretta, E., Bragaglia, A., Gratton, R. G., Recio-Blanco, A., Lucatello, S., D’Orazi, V., & Cassisi, S. 2010, *A&A*, 516, A55+
- Chaboyer, B., Demarque, P., & Sarajedini, A. 1996, *ApJ*, 459, 558
- Charbonnel, C. 2010, in *IAU Symposium*, Vol. 266, IAU Symposium, ed. R. de Grijs & J. R. D. Lépine, 131–142
- De Angeli, F., Piotto, G., Cassisi, S., Busso, G., Recio-Blanco, A., Salaris, M., Aparicio, A., & Rosenberg, A. 2005, *AJ*, 130, 116
- Decressin, T., Baumgardt, H., Charbonnel, C., & Kroupa, P. 2010, *A&A*, 516, A73+
- Decressin, T., Meynet, G., Charbonnel, C., Prantzos, N., & Ekström, S. 2007, *A&A*, 464, 1029
- D’Ercole, A., Vesperini, E., D’Antona, F., McMillan, S. L. W., & Recchi, S. 2008, *MNRAS*, 391, 825
- Fall, S. M. & Zhang, Q. 2001, *ApJ*, 561, 751
- Fan, X., Carilli, C. L., & Keating, B. 2006, *ARA&A*, 44, 415
- Forbes, D. A. & Bridges, T. 2010, *MNRAS*, 404, 1203
- Gratton, R., Sneden, C., & Carretta, E. 2004, *ARA&A*, 42, 385
- Gratton, R. G., Bonifacio, P., Bragaglia, A., Carretta, E., Castellani, V., Centurion, M., Chieffi, A., Claudi, R., Clementini, G., D’Antona, F., Desidera, S., François, P., Grundahl, F., Lucatello, S., Molaro, P., Pasquini, L., Sneden, C., Spite, F., & Straniero, O. 2001, *A&A*, 369, 87
- Griffen, B. F., Drinkwater, M. J., Thomas, P. A., Helly, J. C., & Pimbblet, K. A. 2010, *MNRAS*, 405, 375

- James, G., François, P., Bonifacio, P., Carretta, E., Gratton, R. G., & Spite, F. 2004, *A&A*, 427, 825
- Kalirai, J. S., Strader, J., Anderson, J., & Richer, H. B. 2008, *ApJ*, 682, L37
- Komatsu, E., Smith, K. M., Dunkley, J., Bennett, C. L., Gold, B., Hinshaw, G., Jarosik, N., Larson, D., Nolte, M. R., Page, L., Spergel, D. N., Halpern, M., Hill, R. S., Kogut, A., Limon, M., Meyer, S. S., Odegard, N., Tucker, G. S., Weiland, J. L., Wollack, E., & Wright, E. L. 2011, *ApJS*, 192, 18
- Leitherer, C., Schaerer, D., Goldader, J. D., González Delgado, R. M., Robert, C., Kune, D. F., de Mello, D. F., Devost, D., & Heckman, T. M. 1999, *ApJS*, 123, 3
- Marín-Franch, A., Aparicio, A., Piotto, G., Rosenberg, A., Chaboyer, B., Sarajedini, A., Siegel, M., Anderson, J., Bedin, L. R., Dotter, A., Hempel, M., King, I., Majewski, S., Milone, A. P., Paust, N., & Reid, I. N. 2009, *ApJ*, 694, 1498
- Masters, K. L., Jordán, A., Côté, P., Ferrarese, L., Blakeslee, J. P., Infante, L., Peng, E. W., Mei, S., & West, M. J. 2010, *ApJ*, 715, 1419
- Miralda-Escudé, J., Haehnelt, M., & Rees, M. J. 2000, *ApJ*, 530, 1
- Oesch, P. A., Bouwens, R. J., Carollo, C. M., Illingworth, G. D., Magee, D., Trenti, M., Stiavelli, M., Franx, M., Labbé, I., & van Dokkum, P. G. 2010, *ApJ*, 725, L150
- Ostriker, J. P. & Gnedin, O. Y. 1997, *ApJ*, 487, 667
- Prantzos, N. & Charbonnel, C. 2006, *A&A*, 458, 135
- Prantzos, N., Charbonnel, C., & Iliadis, C. 2007, *A&A*, 470, 179
- Prieto, J. L. & Gnedin, O. Y. 2008, *ApJ*, 689, 919
- Puzia, T. H. & Sharina, M. E. 2008, *ApJ*, 674, 909
- Ricotti, M. 2002, *MNRAS*, 336, L33
- . 2009, *MNRAS*, 392, L45
- Ricotti, M. & Gnedin, N. Y. 2005, *ApJ*, 629, 259
- Ricotti, M. & Shull, J. M. 2000, *ApJ*, 542, 548
- Rosenberg, A., Saviane, I., Piotto, G., & Aparicio, A. 1999, *AJ*, 118, 2306
- Salaris, M. & Weiss, A. 2002, *A&A*, 388, 492
- Sarajedini, A. 2009, in *IAU Symposium*, Vol. 258, *IAU Symposium*, ed. E. E. Mamajek, D. R. Soderblom, & R. F. G. Wyse, 221–232
- Schaerer, D. & Charbonnel, C. 2011, *MNRAS*, 413, 2297
- Shu, C., Luo, Z., Han, M.-A., Chian, A. C.-L., Chen, W.-P., & Wu, Z.-Y. 2010, *Advances in Space Research*, 46, 500
- Snedden, C. 2005, *Highlights of Astronomy*, 13, 149
- Zepf, S. E. & Ashman, K. M. 1993, *MNRAS*, 264, 611
- Zonoozi, A. H., Küpper, A. H. W., Baumgardt, H., Haghi, H., Kroupa, P., & Hilker, M. 2011, *MNRAS*, 411, 1989